Ring to Mountain Transition in Deposition Pattern of Drying Droplets

Xingkun Man[1,2] and Masao Doi[1,2,*]
[1]Center of Soft Matter Physics and its Applications, Beihang University, Beijing 100191, China
[2]School of Physics and Nuclear Energy Engineering, Beihang University, Beijing 100191, China
(Received 15 October 2015; revised manuscript received 25 December 2015; published 9 February 2016)

When a droplet containing a nonvolatile component is dried on a substrate, it leaves a ringlike deposit on the substrate. We propose a theory that predicts the deposit distribution based on a model of fluid flow and the contact line motion of the droplet. It is shown that the deposition pattern changes continuously from a coffee ring to volcanolike and to mountainlike depending on the mobility of the contact line and the evaporation rate. An analytical expression is given for the peak position of the distribution of the deposit left on the substrate.

DOI: 10.1103/PhysRevLett.116.066101

The drying of particle suspensions and polymer solutions gives rise to surprisingly rich deposition patterns [1,2]. The most well known one is the coffee-ring pattern of colloidal suspensions [Fig. 1(a)], where all particles in the droplet are swept to the edge of the droplet. This happens when the contact line is pinned [3,4]. Mountainlike deposits [Fig. 1(b)], which have peaks at the droplet center, have also been reported when the contact line is receding [5–7]. Multiring patterns have been observed when contact lines show stick-slip motion [8–10], and volcanolike patterns [Fig. 1(c)] have also been reported in the drying of polymer solutions [11,12].

Theoretical models have been developed for the drying phenomena of volatile droplets. Previously, most works were limited to the case of a "pinned" contact line. Deegan *et al.* [13] first analyzed the flow induced in a liquid droplet by evaporation and explained the physical origin of the coffee ring. Hu and Larson [14,15] carefully compared the results of flow simulation with experiments and pointed out that the Marangoni effect is important. Such works have further been extended to calculate the profile of the deposit left on the substrate [16–18].

Compared with the case of a pinned contact line, much less work has been done for the case of a moving contact line. Frastia *et al.* [19] have conducted a simulation assuming a concentration dependent viscosity, and have shown that multiring deposition patterns are obtained. Freed-Brown [20] made a simple theory assuming that the contact line can move freely to keep the contact angle at the equilibrium value, and explained the mountainlike deposition pattern. More recently, Kaplan *et al.* [21] proposed a model to interpret the transition of the deposition pattern from uniform films to single rings. All these theories use different models for the motion of the contact line, and our understanding for the deposition pattern in droplets having a moving contact line is still at a primitive stage.

In this Letter, we shall propose a simple model for the drying droplet with a moving contact line, and discuss the change of the deposition pattern (ring to mountain) when the mobility of the contact line and evaporation rate are changed.

We consider a liquid droplet placed on a substrate. Let $R(t)$ be the radius of the base circle of the droplet, and $H(t)$ be the height at the center. We assume that the contact angle is small [$R(t) \gg H(t)$] and therefore the height profile of the droplet $h(r,t)$ at time t is given by a parabolic function

$$h(r,t) = H(t)\left[1 - \frac{r^2}{R^2(t)}\right]. \tag{1}$$

The contact angle is given by $\theta(t) = 2H(t)/R(t)$, and the droplet volume $V(t)$ is

$$V(t) = \frac{\pi}{2} H(t) R^2(t). \tag{2}$$

The volume $V(t)$ of the droplet decreases in time due to solvent evaporation. The evaporation rate of a droplet is

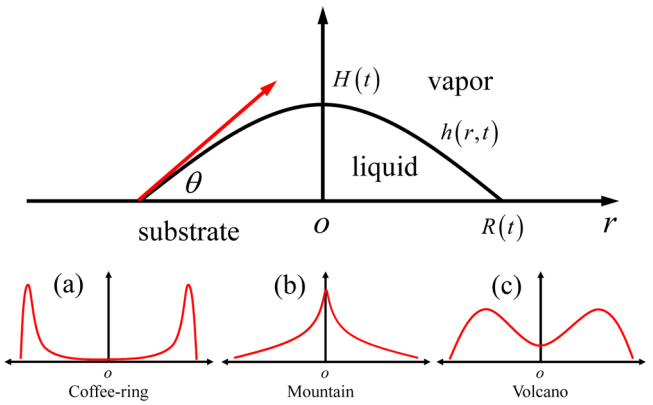

FIG. 1. Schematic of a droplet and three different deposition patterns with axisymmetry in a cylindrical coordinate system (side view). Relevant parameters are the radius of the contact line $R(t)$, the height of the droplet at the center $H(t)$, the contact angle $\theta(t)$, and the profile of liquid-vapor interface $h(r,t)$.

determined by the diffusion of solvent molecules in the gas phase, and can be analyzed theoretically. It has been shown that $\dot{V}(t)$ is proportional to the base radius of the droplet [16,17], and is weakly dependent on the contact angle θ. Here, we ignore the contact angle dependence, and write $\dot{V}(t)$ as

$$\dot{V}(t) = \dot{V}_0 \frac{R(t)}{R_0}, \tag{3}$$

where $\dot{V}_0$ (< 0) and R_0 denote the initial values of $\dot{V}(t)$ and $R(t)$, respectively. $\dot{V}_0$ is expressed in terms of the diffusion constant of the solvent molecules in the gas phase, the solvent vapor pressure near and far from the droplet, and the initial shape of the droplet.

Given the equation for $\dot{V}(t)$, we need one more equation for $\dot{R}(t)$. To determine this, we use the Onsager principle [22–25]. In the current problem, this principle is equivalent to the minimum energy dissipation principle in Stokesian hydrodynamics, which states that the evolution of the system is determined by the minimum of the Rayleighian defined by

$$\Re = \Phi + \dot{F}, \tag{4}$$

where $\dot{F}$ is the time derivative of the free energy of the system, and Φ is the energy dissipation function.

The free energy F is easily obtained. The droplet size is assumed to be less than the capillary length, then the free energy F is written as a sum of the interfacial energy

$$\begin{aligned} F &= (\gamma_{LS} - \gamma_{SV})\pi R^2 + \gamma_{LV} \int_0^R dr 2\pi r \sqrt{1 + h'(r)^2} \\ &= (\gamma_{LS} - \gamma_{SV} + \gamma_{LV})\pi R^2 + \gamma_{LV}\pi H^2, \end{aligned} \tag{5}$$

where γ_{LV}, γ_{LS}, and γ_{SV}, are the interfacial energy density at the liquid-vapor, liquid-substrate, and substrate-vapor interfaces, respectively. Using the equilibrium contact angle $\theta_e = [2(\gamma_{LV} + \gamma_{LS} - \gamma_{SV})/\gamma_{LV}]^{1/2}$, and the volume V of the droplet, Eq. (5) is written as

$$F = \gamma_{LV}\left(\frac{4V^2}{\pi R^4} + \frac{\pi R^2 \theta_e^2}{2}\right). \tag{6}$$

Then, the time derivative of such a free energy is easily obtained as

$$\dot{F} = \gamma_{LV}\left[\left(-\frac{16V^2}{\pi R^5} + \pi\theta_e^2 R\right)\dot{R} + \frac{8V\dot{V}}{\pi R^4}\right]. \tag{7}$$

To calculate the energy dissipation function Φ, we use the lubrication approximation. Let $v(r,t)$ be the height-averaged fluid velocity at position r and time t. The energy dissipation function Φ is written as

$$\Phi = \frac{1}{2}\int_0^R dr 2\pi r \frac{3\eta}{h} v^2 + \pi\xi_{\mathrm{cl}} R\dot{R}^2. \tag{8}$$

The first term represents the usual hydrodynamic energy dissipation (η being the viscosity of the fluid) in the lubrication approximation, while the second term represents the extra energy dissipation associated with the contact line motion over the substrate. Here, ξ_{cl} is a phenomenological parameter representing the mobility of the contact line: ξ_{cl} is infinitely large for a pinned contact line, and is zero for a freely moving contact line. Experiments [6,11] showed that ξ_{cl} originates from the substrate wetting properties, substrate defects, and surface-active solutes. The first two factors affect the hydrodynamic dissipation at the contact line, while the third one affects the surface tension between the liquid and vapor and the liquid and substrate on the molecular scale, resulting in a different receding contact angle, and then it further changes the mobility of the contact line [26].

The velocity $v(r,t)$ in Eq. (8) is obtained from the solvent mass conservation equation

$$\begin{aligned} \frac{d}{dt}\int_0^r dr' 2\pi r' h(r',t) &= -2\pi r v(r,t) h(r,t) \\ &\quad - \int_0^r dr' 2\pi r' J(r',t), \end{aligned} \tag{9}$$

where $J(r,t)$ denotes the evaporation rate (the volume of solvent evaporating per unit time per unit surface area) at position r and time t. It is known that $J(r,t)$ diverges at the contact line in such a way that $J(r,t) \propto [R(t) - r]^{-\frac{1}{2}}$ [3]. However, since this spatial dependence of $J(r,t)$ has a weaker effect compared with the effect of contact line pinning, here we proceed by assuming that $J(r,t)$ is independent of r and has the form

$$J(t) = -\frac{\dot{V}(t)}{\pi R^2(t)} = -\frac{\dot{V}_0}{\pi R_0 R(t)}. \tag{10}$$

Equations (1), (9), and (10) give the following simple expression for $v(r,t)$

$$v(r,t) = r\left(\frac{\dot{R}}{2R} - \frac{\dot{H}}{4H}\right) = r\left(\frac{\dot{R}}{R} - \frac{\dot{V}}{4V}\right). \tag{11}$$

Inserting this expression into Eq. (8), the energy dissipation function Φ is calculated as

$$\Phi = \frac{3\pi^2\eta R^4}{4V}\left[\ln\left(\frac{R}{2\epsilon}\right) - 1\right]\left(\dot{R} - \frac{R\dot{V}}{4V}\right)^2 + \pi\xi_{\mathrm{cl}} R\dot{R}^2, \tag{12}$$

where ϵ is the molecular cutoff length, which is introduced to remove the divergence in the energy dissipation at the contact line. Hereafter, we set $\epsilon = 10^{-6}R_0$ for all calculations.

The Onsager principle states that $\dot{R}$ is determined by the condition $\partial(\Phi + \dot{F})/\partial\dot{R} = 0$. By Eqs. (7) and (12), this gives the following evolution equation

$$(1+k_{\rm cl})\dot{R} = \frac{R\dot{V}}{4V} + \frac{\gamma_{LV}\theta(\theta^2-\theta_e^2)}{6C\eta}, \tag{13}$$

where $C = \ln(R/2\epsilon) - 1$, and $k_{\rm cl}$ is defined by

$$k_{\rm cl} = \frac{\xi_{\rm cl}\theta}{3C\eta}, \tag{14}$$

which characterizes the importance of the extra friction constant $\xi_{\rm cl}$ of the contact line relative to the normal hydrodynamic friction $\xi_{\rm hydro} = 3C\eta/\theta$ [2]. Since not much is known about $\xi_{\rm cl}$, here we proceed making a simple assumption that the ratio $k_{\rm cl} = \xi_{\rm cl}/\xi_{\rm hydro}$ is a constant, or a material parameter determined by the droplet and the substrate.

To simplify the equations, we define two time scales, the evaporation time $\tau_{\rm ev}$ and the relaxation time $\tau_{\rm re}$,

$$\tau_{\rm ev} = \frac{V_0}{|\dot{V}_0|}, \qquad \tau_{\rm re} = \frac{\eta V_0^{\frac{1}{3}}}{\gamma_{LV}\theta_e^3}. \tag{15}$$

The time $\tau_{\rm ev}$ represents the characteristic time for the droplet (of initial size V_0) to dry up, and $\tau_{\rm re}$ represents the relaxation time, the time needed for the droplet (initially having contact angle θ_0) to have the equilibrium contact angle θ_e.

By such a definition, the evolution equation (13) becomes

$$(1+k_{\rm cl})\tau_{\rm ev}\dot{R} = -\frac{V_0R^2}{4R_0V} + \frac{V_0^{\frac{1}{3}}\theta(\theta^2-\theta_e^2)}{6Ck_{\rm ev}\theta_e^3}, \tag{16}$$

where $k_{\rm ev}$ is defined by

$$k_{\rm ev} = \frac{\tau_{\rm re}}{\tau_{\rm ev}}, \tag{17}$$

which is another important parameter characterizing the drying behavior. If $k_{\rm ev}$ is large, the droplet volume decreases much faster than the equilibration of the contact angle θ; therefore, θ becomes much smaller than the equilibrium value θ_e. On the other hand, if $k_{\rm ev}$ is small, θ remains close to θ_e.

For pure water or dilute polymer solutions of macroscopic size (diameter 1 mm), $k_{\rm ev}$ is less than 10^{-3}. On the other hand, for concentrated polymer solutions with high viscosity $k_{\rm ev}$ can be larger than 10^{-1} [27,28].

In Eq. (16), V and θ are functions of time. The evolution of $V(t)$ is given by Eq. (3), which is written as

$$\tau_{\rm ev}\dot{V} = -V_0\frac{R(t)}{R_0}. \tag{18}$$

Finally, θ is related to R and V by

$$\theta = \frac{4V}{\pi R^3}. \tag{19}$$

Equations (16), (18), and (19) are the set of equations that determine the time evolution of our system.

By using the same model, we can calculate the distribution of the deposit left on the substrate. We consider the solute located at position r_0 at time $t = 0$. As the solvent evaporates, such a solute is convected by the fluid. Let $\tilde{r}(r_0,t)$ be the height-averaged position of such a solute at time t. Since the diffusion of the solute in the radial direction can be ignored for macroscopic droplets [29], we can assume that the solute moves with the same velocity as the fluid as long as the solute is in the droplet [i.e., as long as $\tilde{r}(r_0,t) < R(t)$]

$$\dot{\tilde{r}}(r_0,t) = v[\tilde{r}(r_0,t),t] = \left(\frac{\dot{R}}{R} - \frac{\dot{V}}{4V}\right)\tilde{r}(r_0,t) \quad \text{for } \tilde{r}(r_0,t) < R(t). \tag{20}$$

Such a solute will be deposited on the substrate at the time t_d that satisfies $R(t_d) = \tilde{r}(r_0,t_d)$ (notice that t_d defined in this way is a function of r_0). The total amount of solute that was originally contained in the region between r_0 and $r_0 + dr_0$ at time $t = 0$ is $2\pi r_0 h(r_0,0)\phi_0 dr_0$, and this is deposited in the region between $\tilde{r}$ and $\tilde{r} + d\tilde{r}$. Hence, the density of the deposit at the position $\tilde{r}$ is given by

$$\mu[\tilde{r}(r_0,t)] = h(r_0,0)\phi_0\frac{r_0}{\tilde{r}}\left(\frac{d\tilde{r}}{dr_0}\right)^{-1}. \tag{21}$$

Figure 2 shows the deposition density obtained by such a calculation. Here, the initial contact angle θ_0 and the equilibrium contact angle θ_e are taken to be equal to 0.2. Figure 2(a) corresponds to the case of fast evaporation where $k_{\rm ev} = 1$, while Fig. 2(b) corresponds to the case of slow evaporation where $k_{\rm ev} = 10^{-3}$. It is seen that in both cases the peak position shifts inward with the decrease of $k_{\rm cl}$. When $k_{\rm cl} = 100$, the contact line does not move much from the initial position R_0, and the coffee-ring pattern appears. On the other hand, when $k_{\rm cl} = 0$, most solute is accumulated at the center of the droplet, and a mountainlike pattern appears.

Figure 3 shows the peak position r_p of the deposit profile $\mu(r)$ plotted as a function of $k_{\rm cl}$. When $k_{\rm cl}$ is very large, r_p is equal to R_0. As $k_{\rm cl}$ decreases, r_p decreases also. For large values of $k_{\rm ev}$ ($k_{\rm ev} \geq 0.1$), r_p is independent of $k_{\rm ev}$, while for small values of $k_{\rm ev}$ ($k_{\rm ev} < 0.1$), r_p becomes a function of $k_{\rm ev}$.

We can derive an analytical expression for r_p for large values of $k_{\rm ev}$. For $k_{\rm ev} \gg 1$, the second term on the right-hand side of Eq. (13) can be ignored, and the evolution equation for R becomes

$$\dot{R} = \frac{1}{4(1+k_{\rm cl})}\frac{R\dot{V}}{V}. \tag{22}$$

By use of Eqs. (11) and (22), Eq. (20) is written as

$$\dot{\tilde{r}} = -k_{\rm cl}\tilde{r}\frac{\dot{R}}{R}, \tag{23}$$

which is solved as $\tilde{r}(r_0,t) = r_0[R(t)/R_0]^{-k_{\rm cl}}$. The solute initially located at r_0 is deposited at time t_d when $\tilde{r}(r_0,t_d)$

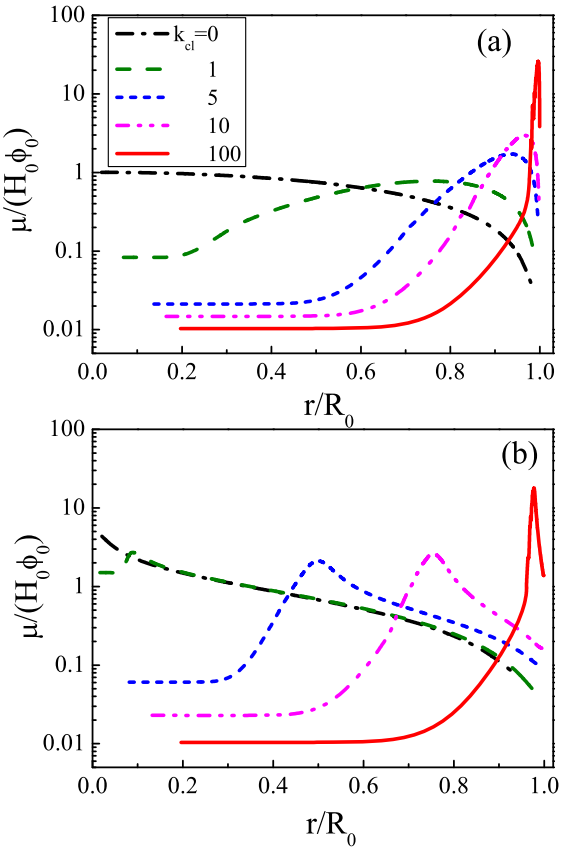

FIG. 2. Profile of the deposit left on the substrate when the drying is completed. The coffee ring to the volcanolike and then to the mountainlike pattern transition induced by changing the value of k_{cl} from 100 to 0. (a) The case of a fast evaporation rate characterized by $k_{\mathrm{ev}} = 1$ and (b) the case that the evaporation rate is small with $k_{\mathrm{ev}} = 10^{-3}$. For both cases, $\theta_e = \theta_0 = 0.2$ and $\Delta t/\tau_{\mathrm{ev}} = 10^{-5}$.

becomes equal to $R(t_d)$, i.e., $r_0[R(t_d)/R_0]^{-k_{\mathrm{cl}}} = R(t_d)$. This gives the following relation between $\tilde{r}(r_0, t_d) = R(t_d)$ and r_0:

$$\tilde{r}(r_0, t_d) = R(t_d) = (r_0)^{\frac{1}{1+k_{\mathrm{cl}}}}(R_0)^{\frac{k_{\mathrm{cl}}}{1+k_{\mathrm{cl}}}}. \tag{24}$$

Inserting Eq. (24) into the expression for μ in Eq. (21), we have

$$\mu(\tilde{r}) = \phi_0 H_0(1 + k_{\mathrm{cl}})\left(\frac{\tilde{r}}{R_0}\right)^{2k_{\mathrm{cl}}}\left[1 - \left(\frac{\tilde{r}}{R_0}\right)^{2(1+k_{\mathrm{cl}})}\right]. \tag{25}$$

By maximizing $\mu(\tilde{r})$ with respect to $\tilde{r}$, we have an explicit expression for the peak position r_p

$$r_p = R_0\left(\frac{k_{\mathrm{cl}}}{2k_{\mathrm{cl}} + 1}\right)^{\frac{1}{2(1+k_{\mathrm{cl}})}}. \tag{26}$$

This curve is shown by the black solid line in Fig. 3, which agrees quite well with the numerical results. When

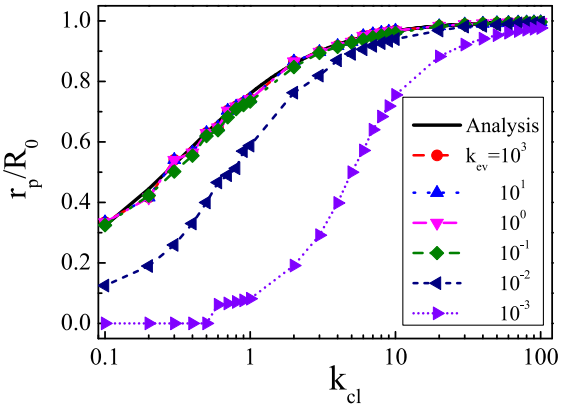

FIG. 3. The peak position r_p of the deposit density distribution is plotted against k_{cl}. The results of the numerical calculation for various values of k_{ev} are denoted by symbols, while the analytical result (26) is denoted by the black-solid line. All other parameters are the same as in Fig. 2.

$k_{\mathrm{cl}} \gg 1$, r_p approaches R_0, giving the coffee-ring pattern (Deegan's limit), while when $k_{\mathrm{cl}} \ll 1$, r_p goes to zero, leading to the mountainlike deposition (Freed-Brown's limit). Equation (26) smoothly interpolates these two limits.

As seen in Fig. 3, the curve r_p/R_0 vs k_{cl} starts to deviate from the analytical formula (26) for $k_{\mathrm{ev}} \leq 10^{-2}$. This deviation can be understood by looking at the droplet shape during drying.

Figure 4 shows the time evolution of droplet shape and deposition pattern for both fast evaporation ($k_{\mathrm{ev}} = 1$) and slow evaporation ($k_{\mathrm{ev}} = 10^{-3}$) [30]. When the evaporation rate is fast, the solvent is taken out from the surface of the droplet, inducing a large deformation of the droplet. Hence, the contact angle $\theta(t)$ decreases in time, while the contact radius $R(t)$ remains almost constant [Fig. 4(a)]. As a result, the deposit peak appears near R_0 [Fig. 4(b)]. On the other hand, when the evaporation rate is slow, a fluid flow is induced to maintain the equilibrium contact angle. Accordingly, the contact radius $R(t)$ decreases in time [Fig. 4(c)], and the deposit peak appears inside the original contact area [Fig. 4(d)].

Since there is no quantitative study about the relation between the drying condition and the deposition pattern, it is difficult to make a quantitative comparison between the theory and experiments. However, a qualitative comparison can be made. Li *et al.* [6] studied various solution droplets placed on different substrates, and observed the transition of the deposition pattern from a coffee ring to mountainlike. With a weak contact angle hysteresis substrate (like a silica glass or polycarbonate substrate for the water droplet), the contact line recedes and forms the mountainlike deposition patterns. On the other hand, for a strong contact angle hysteresis substrate (like graphite), the contact line is pinned and leaves coffee-ring patterns. These observations are in agreement with the present theory. Kajiya *et al.* [11] studied the drying of a water-poly(N,N-dimethylacrylamide) PDMA

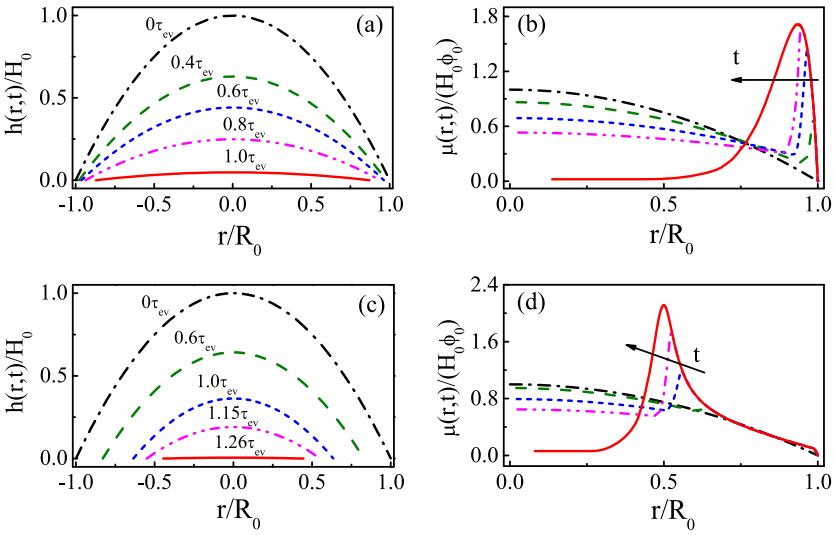

FIG. 4. Evolution of the profile of the droplet's interface between the liquid and vapor, $h(r,t)/H_0$, and solute density distribution $\mu(r,t)/(H_0\phi_0)$ for (a), (b) a fast evaporation rate $k_{ev} = 1$, and for (c), (d) a slow evaporation rate $k_{ev} = 10^{-3}$. In all figures, the black dash-dot line represents the initial state, while the red solid line is the final state after drying up. The time steps in (b) and (d) are the same as in (a) and (c), accordingly. The arrow is the direction of the time evolution of the drying process. Other parameters are $k_{cl} = 5$, $\theta_e = \theta_0 = 0.2$, and $\Delta t/\tau_{ev} = 10^{-5}$.

droplet on a glass substrate and observed volcanolike deposition patterns. They have explained the volcanolike pattern based on the mobility of the contact line, which is also consistent with our theory.

In this Letter, we have proposed a simple model for a drying droplet that accounts for the contact line motion and the solvent evaporation simultaneously. We have clarified how the contact line friction (described by k_{cl}) and the evaporation rate (described by k_{ev}) affect the final deposition pattern, especially the transition from coffee ring to volcanolike and then to mountainlike patterns. What remains to be done is to include a stick-slip mechanism in the model to capture the multiring phenomena and other more interesting deposition patterns.

This work was supported in part by Grants No. 21404003, No. 21434001 and No. 51561145002 from the National Natural Science Foundation of China (NSFC), and the Fundamental Research Funds for the Central Universities.

*masao.doi@buaa.edu.cn

[1] R. D. Deegan, Phys. Rev. E **61**, 475 (2000).
[2] D. Bonn, J. Eggers, J. Indekeu, J. Meunier, and E. Rolley, Rev. Mod. Phys. **81**, 739 (2009).
[3] R. D. Deegan, O. Bakajin, T. F. Dupont, G. Huber, S. R. Nagel, and T. A. Witten, Nature (London) **389**, 827 (1997).
[4] Á. G. Marín, H. Gelderblom, D. Lohse, and J. H. Snoeijer, Phys. Rev. Lett. **107**, 085502 (2011).
[5] D. Willmer, K. A. Baldwin, C. Kwartnik, and D. J. Fairhurst, Phys. Chem. Chem. Phys. **12**, 3998 (2010).
[6] Y.-F. Li, Y.-J. Sheng, and H.-K. Tsao, Langmuir **29**, 7802 (2013).
[7] Y.-F. Li, Y.-J. Sheng, and H.-K. Tsao, Langmuir **30**, 7716 (2014).
[8] Z. Q. Lin and S. Granick, J. Am. Chem. Soc. **127**, 2816 (2005).
[9] J. Xu, J.-F. Xia, S. W. Hong, Z.-Q. Lin, F. Qiu, and Y.-L. Yang, Phys. Rev. Lett. **96**, 066104 (2006).
[10] S. Maheshwari, L. Zhang, Y.-X. Zhu, and H.-C. Chang, Phys. Rev. Lett. **100**, 044503 (2008).
[11] T. Kajiya, C. Monteux, T. Narita, F. Lequeux, and M. Doi, Langmuir **25**, 6934 (2009).
[12] K. Fukuda, T. Sekine, D. Kumaki, and S. Tokito, ACS Appl. Mater. Interfaces **5**, 3916 (2013).
[13] R. D. Deegan, O. Bakajin, T. F. Dupont, G. Huber, S. R. Nagel, and T. A. Witten, Phys. Rev. E **62**, 756 (2000).
[14] H. Hu and R. G. Larson, J. Phys. Chem. B **106**, 1334 (2002).
[15] H. Hu and R. G. Larson, Langmuir **21**, 3963 (2005).
[16] F. Parisse and C. Allain, Langmuir **13**, 3598 (1997).
[17] M. Kobayashi, M. Makino, T. Okuzono, and M. Doi, J. Phys. Soc. Jpn. **79**, 044802 (2010).
[18] T. Okuzono, M. Kobayashi, and M. Doi, Phys. Rev. E **80**, 021603 (2009).
[19] L. Frastia, A. J. Archer, and U. Thiele, Phys. Rev. Lett. **106**, 077801 (2011).
[20] J. Freed-Brown, Soft Matter **10**, 9506 (2014).
[21] C. N. Kaplan and L. Mahadevan, J. Fluid Mech. **781**, R2 (2015).
[22] T.-Z. Qian, X.-P. Wang, and P. Sheng, J. Fluid Mech. **564**, 333 (2006).
[23] M. Doi, J. Phys. Condens. Matter **23**, 284118 (2011).
[24] M. Doi, *Soft Matter Physics* (Oxford University Press, New York, 2013).
[25] M. Doi, Chin. Phys. B **24**, 020505 (2015).
[26] J. H. Snoeijer and B. Andreotti, Annu. Rev. Fluid Mech. **45**, 269 (2013).
[27] T. Kajiya, W. Kobayashi, T. Okuzono, and M. Doi, J. Phys. Chem. B **113**, 15460 (2009).
[28] T. Kajiya, W. Kobayashi, T. Okuzono, and M. Doi, Langmuir **26**, 10429 (2010).
[29] D. M. Anderson and S. H. Davis, Phys. Fluids **7**, 248 (1995).
[30] See Supplemental Material at http://link.aps.org/supplemental/10.1103/PhysRevLett.116.066101 for movies of the temporal evolution of droplet shape (light blue) and solute density distribution (red) for both fast evaporation rate and slow evaporation rate cases.